Contrib Mineral Petrol (2007) 153:577–591
DOI 10.1007/s00410-006-0163-7

ORIGINAL PAPER

Formation of Pt, Pd and Ni tellurides: experiments in sulfide–telluride systems.

Hassan M. Helmy · Chris Ballhaus · Jasper Berndt · Cornelia Bockrath · Cora Wohlgemuth-Ueberwasser

Received: 26 June 2006 / Accepted: 8 November 2006 / Published online: 12 December 2006

Abstract We evaluate experimentally the role of temperature and metal/Te ratio on the composition and crystallization temperature of sulfides and tellurides in the Fe–Cu–Ni–Pd–Pt–Te–S system. The monosulfide–sulfide melt partition coefficients decrease with increasing Te concentration and decreasing S/Te ratio of the bulk composition because Pt and Pd are strongly complexed by Te and thus stabilized in the melt phase. The solubility of Te in Fe-rich monosulfide solid solution and Cu-rich intermediate solid solution is around 0.2 wt% and largely insensitive to temperature down to 320°C, indicating that Te substitutes in sulfides as an anion replacing S. Solid solution between moncheite $PtTe_2$ and merenskyite $PdTe_2$ is more limited than implied by natural telluride phase compositions. Solid solution between tellurides with variable metal/Te stoichiometry also appears to be limited, again in contrast to natural phase compositions. Natural tellurides are compositionally more flexible than the experimental compositions synthesized here. It is argued, therefore, that many natural tellurides coexisting with sulfides may be metastable, i.e. modified by exsolution of a Ni–Te component from the coexisting high-temperature sulfides. From Te concentrations in monosulfide solid solution it is deduced that natural sulfide–telluride assemblages record equilibration temperatures as low as 200–250°C. With respect to Te and precious metal mineralization, no systematic temperature difference exists between sulfide–telluride ores referred to in the descriptive ore petrography literature as magmatic and ores termed hydrothermal in origin.

Communicated by J. Hoefs.

H. M. Helmy
Geology Department, Faculty of Science,
El-Minia University, El-Minia, Egypt

C. Ballhaus (✉)
Mineralogisches Institut und Museum, Universität Bonn,
Poppelsdorfer Schloss, 53115 Bonn, Germany
e-mail: ballhaus@uni-bonn.de

J. Berndt · C. Wohlgemuth-Ueberwasser
Institut für Mineralogie, Universität Münster,
48149 Münster, Germany

C. Bockrath
Landesmuseum Kärnten, Museumgasse 2,
9021 Klagenfurt, Austria

Introduction

Telluride-bearing sulfide ore is not only the main repository for the rare elements Te, Sb, and Bi; telluride minerals also are important carriers of precious metals, especially of Pt, Pd, Au, and Ag. Tellurides are stable in a wide variety of geological environments. For example, in the Merensky reef of the Bushveld Complex, the most important magmatic deposit for platinum-group elements (PGE), Pt and Pd tellurides comprise about 20% of the modal abundance of platinum group minerals (Cawthorn et al. 2002), and in the Platreef it can be more than 50% (Holwell and McDonald 2006). In the Ni sulfide ores of the Sudbury intrusion, Pd is an important byproduct, and Pd occurs to a large extent as bismuthotelluride minerals (Cabri and Laflamme 1976; Naldrett 2004). Te is the only ligand in nature that forms stable compounds with Au, notably in epithermal porphyry-style mineralizations at

convergent plate margins, and a large proportion of the precious metals in these types of mineralizations occur as intermetallic compounds with the semi-metals Te and Bi (cf. Tarkian and Koopmann 1995). Therefore, it is of interest to the ore petrologist, to understand how elements like Te influence magmatic differentiation of sulfide melt and at what temperatures telluride–sulfide mineral assemblages commonly form.

The most common natural Pt and Pd tellurides are moncheite $PtTe_2$, merenskyite $PdTe_2$, melonite $(Ni,Pd)Te_2$ and kotulskite (Pd,Ni)Te. In addition, there are the bismuthotellurides michenerite PdTeBi, sobolevskite Pd(Bi,Te), maslovite (Pt,Pd)BiTe, Sb-bearing tellurides like borovskite Pd_3SbTe_4, and many other less common phases. Usually, Pt–Pd bismuthotellurides occur together with magmatic Fe–Ni–Cu sulfide mineralizations. The descriptive ore petrography literature distinguishes between magmatic and hydrothermal sulfide–telluride ores. In sulfide–telluride assemblages interpreted as magmatic (Mulja and Mitchell 1991; Helmy and Mogessie 2001), moncheite and merenskyite occur as inclusions in, or in close association with, the low-temperature recrystallization products of monosulfide solid solution (mss), i.e. pyrrhotite, pentlandite, and chalcopyrite (Garuti and Rinaldi 1986; Helmy 2005). Extensive substitution of Pd by Pt and Te by Bi in telluride phases is also taken as chemical evidence for an elevated crystallization temperature. For example, based on Bi and Pd concentrations in moncheite from the Upper Section of the Keivitsansarvi Ni–Cu–PGE deposit, Gervilla and Kojonen (2002) suggested a crystallization temperature in excess of 750°C. Barkov et al. (1999) postulated that bismuthian merenskyite from the Mount General Skaya intrusion crystallized at >600°C, and Helmy et al. (1995) derived from the compositions of coexisting merenskyite and michenerite at the Abu Swayel Cu–Ni–PGE prospect a temperature of 475°C. Telluride inclusions in high temperature silicates or oxides, which could be taken as fairly robust evidence for a magmatic origin of these phases, have not yet been reported.

In contrast, in what is often referred to as hydrothermal ore, the tellurides either occur at the sulfide–silicate interface or they are hosted in mobilized chalcopyrite, violarite, and secondary hydrous silicates (Rowell and Edgar 1986; Helmy et al. 1995; Barkov et al. 1999, 2002; Gervilla and Kojonen 2002). Temperatures here are thought to range from 540 to <350°C (Farrow and Watkinson 1992; Magyarosi et al. 2002; Helmy 2004). Estimates are based on phase equilibria among coexisting sulfide, oxide, silicate, and telluride mineral assemblages (e.g. Barkov et al. 1999; Magyarosi et al. 2002).

But how realistic are these temperature estimates? Is it justified to derive temperature conditions from textures and phase compositions? For example, tellurides deemed magmatic occur with sulfides like pyrrhotite, pentlandite, chalcopyrite, and pyrite, which are by no means magmatic but form by reaction between, and exsolution of, mss and intermediate solid solution (iss) at temperatures <300°C (e.g. Craig 1973; Misra and Fleet 1973; Kaneda et al. 1986; Naldrett 2004; Etschmann et al. 2004). Pyrrhotite in so-called magmatic sulfide ore is essentially Ni-free (typically ~0.2 wt%), and although the Ni content in pyrrhotite in equilibrium with pentlandite was never calibrated quantitatively as a thermometer, it is clear that these low levels in Ni record closure temperatures not more than 150–200°C (Ballhaus and Ryan 1995). Perhaps it is reasonable to say that the textures in magmatic sulfide–telluride ore might be magmatic, owing to the lack of overprint by hydrous alteration or deformation, however, the sulfide assemblages and the sulfide phase compositions are not magmatic. Nor is it well established that we can use telluride compositions as thermometers. For ores termed hydrothermal, the situation is not much better. Evidently, these types of ores record hydrothermal overprints, but there is no convincing parameter that would allow temperatures to be quantified or PGE–Bi–Te mineralization to be related to fluids.

We have equilibrated Pt–Pd tellurides and $(Fe, Ni, Cu)_{1-x}S$ sulfides over a wide range of temperatures from magmatic to hydrothermal. All tellurides were synthesized in the presence of Fe–Ni–Cu base metal sulfides, the rationale being that a Pt–Pd telluride mineral can coexist with base metal sulfides only if the sulfides themselves are saturated with Pt, Pd, and Te. We observe that the Te concentration in FeS-rich sulfides is independent of temperature, at least down to 370°C, and typically around 0.2 wt%. No natural FeS-rich sulfide coexisting with Pt–Pd telluride phases is known to reach such levels of Te concentration. It appears, therefore, that in terms of equilibration temperature, there is no difference between a magmatic and a hydrothermal sulfide–telluride ore.

Natural phase compositions and previous investigations

Solid solutions are known to occur between all members of the Pt, Pd and Ni tellurides. The most important solid solutions are between melonite and merenskyite (Rucklidge 1969), Ni-poor merenskyite and moncheite (Cabri and Laflamme 1976), and between melonite and moncheite (Hudson 1986).

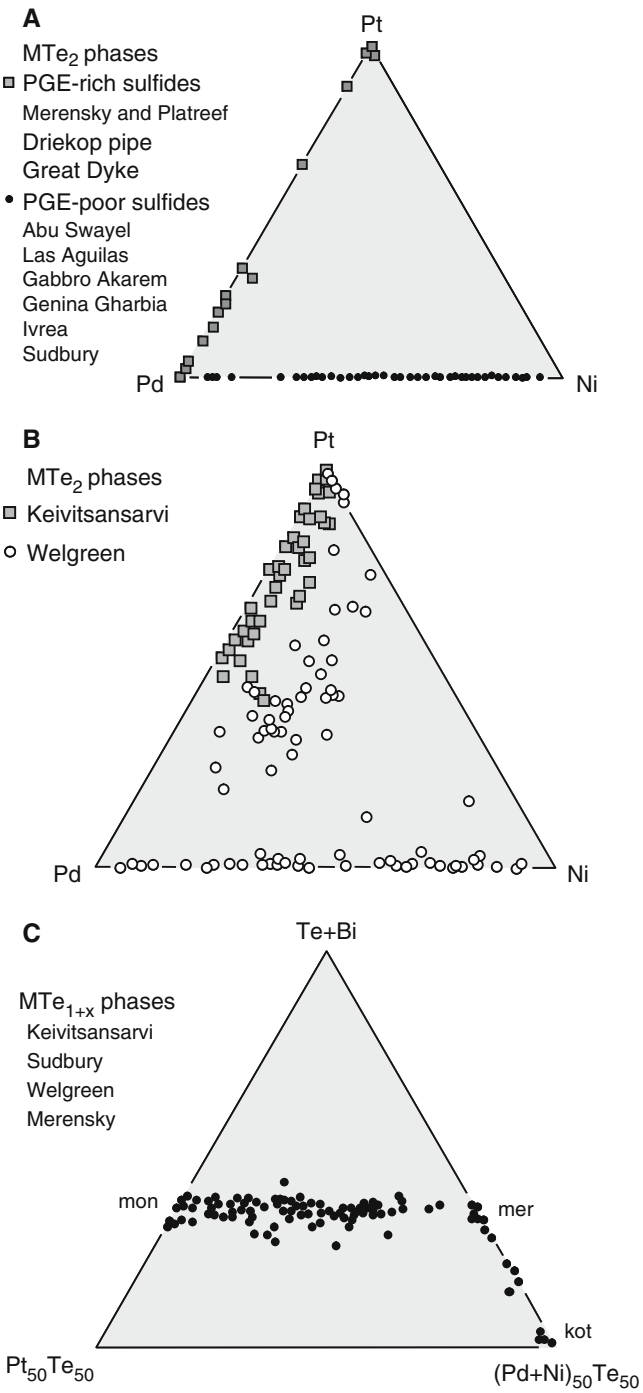

Fig. 1 Natural telluride phase compositions in Fe–Ni–Cu sulfide mineralizations (Te/Bi + Sb) atomic ratio > 1. **a** Ni-free telluride compositions from the PGE-rich ores of the Bushveld and Great Dyke complexes, and Pt-free tellurides from a number of PGE-poor sulfide deposits. **b** Telluride compositions in ternary space, some of which may be metastable with respect to their $NiTe_2$ component (see text). **c** Tellurides with variable PGE/semimetal ratios in the Pt – (Pd + Ni) – (Te + Sb + Bi) ternary space. Sources: Merensky reef (Pt-rich tellurides; Kingston and Eldosuky 1982; Prichard et al. 2004), Platreef (Pd-rich bismuthotellurides; courtesy D. Holwell 2006), Hartley platinum mine, Great Dyke (Pt-dominated bismuthotellurides; Oberthür et al. 2003), Driekop pipe, Bushveld Complex (Pt bismuthotellurides; Melcher and Lodziak 2006), Abu Swayel, Gabbro Akarem, Genina Gharbia, Egypt (Helmy 2005), Las Aguilas, Argentina (Gervilla et al. 1997), Wellgreen, Yukon Territory (Barkov et al. 2002), Keivitsansarvi, Finland (Gervilla and Kojonen 2002), Sudbury (Cabri and Laflamme 1976)

Figure 1a and b show the compositional variability of tellurides with a metal/semimetal 1:2 stoichiometry, i.e., the phases of the melonite-group, from a wide variety of occurrrences with and without hydrothermal overprint. Many of the phases in Fig. 1a and b contain, in addition, some Bi and Sb replacing Te, but Bi and Sb-dominated phases were not considered for inclusion in the diagram since our experimental compositions did not contain Bi or Sb.

Provided the diagrams represent equilibrium compositions (see below), there appears to be complete solid solution along the $PdTe_2$–$NiTe_2$ (merenskyite–melonite) join. Many sulfide deposits, notably those poor in PGE (Fig. 1a), only contain telluride phases along that join. Extensive miscibility is also noted along the binary $PtTe_2$–$PdTe_2$ moncheite–merenskyite join. Along this join fall tellurides from very PGE-rich sulfide ores like the Merensky reef and the Platreef of the Bushveld Complex, and possibly from the stratiform PGE horizons in the Great Dyke, Zimbabwe (Oberthür et al. 2003). Solid solution along the $PtTe_2$–$NiTe_2$ (moncheite–melonite) binary appears to be more limited, the only examples being a few Ni-bearing moncheites from the Welgreen deposit in Canada (Barkov et al. 2002). In the ternary space, however, miscibility is enhanced, perhaps aided by semimetals like Sb and Bi replacing Te. The telluride compositions from the Welgreen deposit appear to be bimodal with respect to $PtTe_2$ contents, and as such they may outline a miscibility gap in the pseudoternary $(Pt,Pd,Ni)Te_2$ space. Note, however, that there are no experimental data on $(Pt,Pd,Ni)Te_2$ to substantiate this, or that the natural variations are indeed equilibrium compositions. In the following, we speculate that many of the ternary $PtTe_2$–$PdTe_2$–$NiTe_2$ solid solutions may be metastable, i.e., modified by subsolidus exsolution of a $NiTe_2$ component from sulfide and its precipitation on pre-existing Pt–Pd tellurides.

In addition to variations in Pt, Pd, and Ni, tellurides may also vary in terms of metal–Te stoichiometry. From the distribution of phase compositions in Fig. 1C, it appears that solid solution between MTe and MTe_2 stoichiometries is quite pronounced, if not complete, but note that all MTe_{1+x} compositions intermediate between merenskyite and kotulskite come from one

deposit (Welgreen; Barkov et al. 2002) with a very complex bismuthotelluride mineralogy. Experiments also suggest that solid solution along the PdTe–$PdTe_2$ join is extensive. Medvedeva et al. (1961) noted complete solid solution above 640°C between kotulskite (PdTe) and merenskyite ($PdTe_2$), and Hoffman and MacLean (1976), studying the Pd–Bi–Te system, reported complete PdTe–$PdTe_2$ miscibility above 575°C. Kim and Chao (1991) observed kotulskite–merenskyite myrmekitic intergrowths in experiments in the Pd–Sb–Te system quenched from 600°C, and interpreted these intergrowths as exsolutions from originally homogenous crystalline $PdTe_{1+x}$ intermetallic compounds. No natural Pt-rich telluride with M/Te (1:1) stoichiometry is known, and accordingly solid solution in ternary space is limited. Part of the scatter about the $PtTe_2$–$PdTe_2$ join in Fig. 1c could probably be attributed to analytical variations or small-scale phase heterogeneities.

Experimental and analytical procedures

Because Pt–Pd–Ni tellurides are often associated with base-metal sulfides, phase equilibria in telluride systems were studied in the presence of Fe–Ni–Cu sulfides. In the experiments reported here, the telluride compositions were synthesized in an $(Fe,Ni,Cu)_{1-x}S$ monosulfide matrix (sulf-1 in Table 1) and equilibrated between 1,150 and 320°C. Two sets of experiments were performed with two different telluride stoichiometries in sulfide; a Te-rich telluride component with a (Pt + Pd + Ni)/Te atomic ratio of 0.5, and a metal-rich telluride component with a (Pt + Pd)/Te atomic ratio of 0.65 (Table 1). By varying the metal/Te ratio, we aimed to stabilize in the charges tellurides with different metal/Te stoichiometries. In addition, one experiment at low temperature (HH42, 320°C) used a Ni-enriched sulfide component as matrix (sulf-2 in Table 1), to promote the crystallization of melonite in addition to Pt–Pd tellurides. However, in terms of phase equilibria, this composition yielded results largely identical to those obtained with the relatively Ni-poor sulfide component.

The sulfide and telluride starting mixes were synthesized from pure metal powders, elemental S and Te. Starting mixes were welded in evacuated SiO_2 glass tubes and reacted stepwise to sulfide or telluride assemblages for about 24 h at 200, 300, 500, and finally 700°C. To keep out oxygen, the tubes were repeatedly flushed with Ar before final evacuation.

Each experiment used 100 mg of sulfide and 15 mg of either the Te-rich or metal-rich telluride component. The mixtures were welded under high vacuum in 6 mm SiO_2 glass tubes. The tubes were suspended on a retractable Pt wire inside the hot zone of a vertical quench furnace. For each experiment, the charge was melted at 1,150°C for 30 min, cooled to the designated run temperature by 30°C per hour, kept there for the designated run time, and then quenched by releasing the tube in cold water. Experiments at <700°C were carried out in conventional muffle ovens and quenched manually in cold water, because the supercantal heating elements of our vertical ovens do not tolerate a temperature of <700°C for extended periods of time. In both setups, temperatures were controlled with $PtRh_5$–$PtRh_{30}$ thermocouples to within ±5°C calibrated on the melting point of gold. Table 2 summarizes the experimental conditions and phase relations.

Phase relations with the Te-rich telluride component (metal/Te = 0.5)

Backscattered electron images of selected run products are illustrated in Fig. 2. The 1,000°C charge, our highest temperature experiment with the Te-rich telluride, was completely molten. Metastable quench products are dendritic mss, Ni–Cu-enriched iss, and irregular patches of telluride. The telluride quench patches are distributed evenly inside the sulfide matrix, suggesting that above 1,000°C, telluride and sulfide melts are fully miscible in the proportions they were added to the charge.

Table 1 Starting sulfide and telluride compositions

	Sulfide matrices		Telluride components	
	Sulf-1	Sulf-2	Te-rich	Metal-rich
Weight %				
Fe	40.4	29.7	–	–
Ni	15.6	31.4	5.5	–
Cu	7.7	4.6	–	–
Pd	–	–	9.5	15.4
Pt	–	–	17.3	28.2
Te	–	–	67.7	56.4
S	36.3	34.3	–	–
Atomic %				
Fe	32.3	24.1	–	–
Ni	11.8	24.2	11.4	–
Cu	5.4	3.3	–	–
Pd	–	–	11	19.8
Pt	–	–	11	19.7
Te	–	–	66.6	60.5
S	50	48.4	–	–
Metal/S	0.99	1.07	–	–
Metal/Te	–	–	0.5	0.65

At 900°C, mss and moncheite are stable crystalline phases and coexist with sulfide melt and telluride melt (Fig. 2a). Monosulfide tends to form rounded grains up to 250 μm in diameter, set in a matrix of Cu–Ni-enriched melt. Moncheite forms elongate crystals attached to, or immersed in, pools of Pd-enriched telluride melt that quenched to metastable (Pd,Ni,Pt)Te_{1+x} compositions. The distribution of telluride in sulfide is patchier and more irregular than in the 1,000°C run. This observation, plus the fact that moncheite invariably occurs in contact with quenched Pd-rich telluride melt, suggest that at 900°C, sulfide melt and telluride melt are not fully miscible any more.

At 700°C, monosulfide grains have increased in size and have become more abundant. Mss now coexists with stable equilibrium iss (Fig. 2b, c). At this temperature, the amount of interstitial sulfide melt is only a few percent. Compared to the higher temperature runs, the sulfide melt is richer in Cu and quenches to iss and Cu_2S, consistent with the fact that Cu is moderately incompatible with mss (Ballhaus et al. 2001). Elongate, sometimes needle-shaped moncheite still is the only stable crystalline telluride, again rimmed by telluride melt that quenched to metastable (Pd,Ni,Pt)Te_{1+x} (Fig. 2c). In addition, grain contacts between mss and iss are decorated with tiny Pd–telluride grains, possibly the crystallization products of thin films of telluride melt, wetting sulfide grain boundaries at run conditions.

At 600°C, sulfide melt is consumed. Stable sulfides are mss and iss. Tellurides form aggregates inside iss and consist of moncheite with attached merenskyite (Pd,Ni,Pt)Te_2. At 600°C and at lower temperature, we note chemical zonation with respect to Pt and Pd across moncheite–merenskyite grain contacts (Fig. 2d). The Pd-rich telluride is much poorer in Pt than equivalent (Pd,Ni,Pt)Te_{1+x} phases in the higher temperature runs and therefore interpreted to be crystalline at 600°C. In the 500°C run, we note that Pt–Pd zonation has increased, to an extent that contacts between moncheite and merenskyite can be completely blurred. Perhaps this type of telluride zonation originated in the initial cooling phase of the experiment: As mentioned above, all experiments were initially heated to 1,150°C, then cooled slowly by 30°C per hour to the designated run temperature, and this means that the solidus of the Pd–Te-rich telluride melt may have been crossed during this initial cooling phase, before the actual run temperature was reached. If this interpretation is correct, the solidus of the Te-rich telluride charge must lie above 600°C.

At 400°C, Pt/Pd telluride zonation toward moncheite still persists. Only in the lowest temperature run, at 320°C, do the contacts between moncheite and the (Pd,Ni,Pt)Te_2 phase become distinct again. This 320°C temperature run was kept for nearly 5 months, and maybe time was sufficient to even out chemical zonation by solid-state diffusion. At 320°C, two crystalline tellurides are stable, i.e. moncheite with close to end-member composition coexisting with merenskyite. Interestingly, no discrete Ni tellurides were found in this run even though both the sulfide and the telluride components were enriched with extra Ni; in fact merenskyite is lower in Ni in that Ni-enriched charge

Table 2 Summary of experimental conditions and run products

Run	*T* (°C)	Run time (*h*)	Run products
Set 1, experiments with Te-rich telluride			
HH41	1,000	6	Superliquidus (Te-bearing sulfide melt)
HH40	900	12	mss + mon + sulfide melt + telluride melt
HH21	700	96	mss + iss + mon + sulfide melt + telluride melt
HH27	600	180	mss + iss + mon + mer
HH28	500	384	mss + iss + mon + mer
HH26	400	480	mss + iss + mon + mer
HH42[a]	320	4,320	mss + pent + iss + mon + mer
HH23[b]	500	312	mss + iss + mon + mer
HH24[b]	400	408	mss + iss + mon + mer
Set 2, experiments with metal-rich telluride			
HH5	1,150	0.5	Superliquidus (Te-bearing sulfide melt)
HH3	1,015	4	mss + sulfide melt + telluride melt
HH4	920	6	mss + iss + mon + sulfide melt + telluride melt
HH2	825	20	mss + iss + mon + telluride melt
HH6	725	60	mss + iss + mon + telluride melt
HH1	625	60	mss + iss + mon + kot
HH10	500	360	mss + iss + mon + kot
HH11	370	720	mss + iss + mon + kot + unknown Pd_3Te_2 phase

mss monosulfide solid solution, *iss* intermediate solid solution, *pent* pentlandite, *mon* moncheite, *mer* merenskyite, *kot* kotulskite

[a] HH42 with Ni-rich sulfide matrix (sulf-2 in Table 2), all other experiments with sulf-1

[b] Reversed experiments

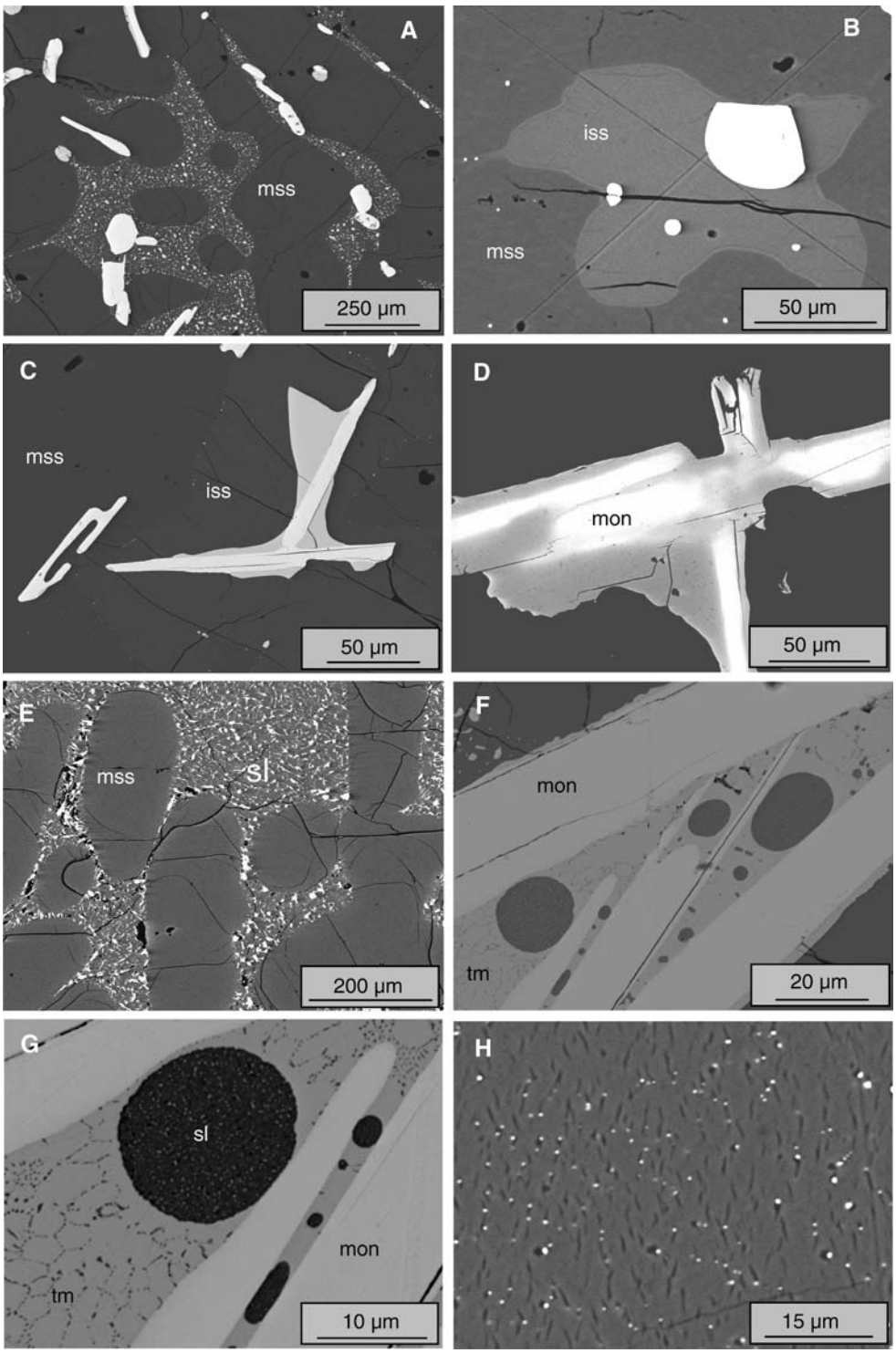

Fig. 2 BSE images of run products (experiments with both the Te-rich and the metal-rich telluride component). **a** Mss coexisting with bright telluride phases (moncheite with attached Pd telluride melt) plus sulfide melt (900°C). **b** Mss and iss coexisting with bright Pd-rich telluride phases (825°C). **c** White moncheite needles with attached quenched (*gray*) Pd-rich telluride melt, both embedded in iss (700°C). **d** Moncheite (*mon*) with attached merenskyite (*mer*) in iss matrix (600°C); note the blurred contact between moncheite and merenskyite, a feature that becomes more pronounced in the lower temperature runs. **e** Rounded grains of monosulfide solid solution (*mss*) set in quenched sulfide melt (*sl*); sulfide melt exsolves upon quenching small telluride melt aggregates (1,015°C). **f** Pd-rich telluride melt (*tm*) with droplets of an immiscible Cu-rich sulfide melt, wedged between moncheite laths; dark phase in lower right and upper left is iss (920°C). **g** Same as **f** but in more detail and more contrast; the telluride melt (*tm*) quenched to roundish Pd–Te phases and small (*dark*) sulfide grains decorating the grain boundaries of quench Te phases, the sulfide melt (*sl*) quenched to dark Cu-rich sulfide with tiny specs of Pd-rich telluride. **h** Detail of an mss grain with subsolidus Cu-rich exsolution rods; note the white Pd–Te inclusions concentrated together with the iss exsolution lamellae (825°C)

than in the other runs. At 320°C, a Ni-enriched pentlandite is stable in addition to pyrrhotite and a Cu-rich phase approaching the composition of chalcopyrite. That phase was found so densely impregnated with tiny Pd-rich telluride inclusions that contamination-free EMP analyses were difficult to obtain.

Phase relations with metal-rich telluride (PGE/Te = 0.65)

At 1,150°C, both sulfide and telluride charges are at superliquidus conditions. Quench phases are dendritic FeS-rich mss, Cu–Ni-rich iss, and fine speckles of telluride,

wedged between sulfide quench crystals. At this temperature and sulfide/telluride weight ratio (15 wt% telluride), sulfide and telluride seem to be fully miscible. At 1,015°C, stable phases are rounded mss, quenched Cu–Ni-rich sulfide melt, and patches of quenched telluride melt (Fig. 2e). The telluride is always situated in quenched sulfide melt, forming larger aggregates than in the superliquidus 1,150°C run. At high magnification, the telluride patches are heterogeneous with respect to Pt/Pd, showing myrmekitic internal structures and micron-sized needles of quench moncheite sitting in Pd-rich telluride matrix. An even distribution of telluride in quenched sulfide melt suggests that at this temperature, sulfide and telluride melts still are fully miscible.

At 920°C, mss is joined by moncheite and iss as stable equilibrium phases, coexisting with immiscible Cu-rich sulfide and Pd-enriched telluride melts (Fig. 2f, g). At 825°C, the sulfide melt appears to be completely consumed. The only melt phase stable at this temperature is a Pd-rich telluride melt, always wetting moncheite laths. Mss starts to exsolve rodlets of a Cu-rich sulfide that is speckled with tiny telluride grains (Fig. 2h). At 725°C, the exsolutions have become coarser and more abundant. The Pd-rich telluride phase wetting the moncheite laths now approaches a metal/Te atomic ratio close to that of kotulskite, but based on grain shapes, we consider it still molten. At 625°C, all melt phases have disappeared. Kotulskite (Pd,Pt,Ni)Te is a crystalline phase and forms euhedral stubby crystals intergrown with moncheite. Stable sulfides are mss and iss. Not much change is noted at 500°C. Finally, at 370°C, our lowest temperature experiment with the metal-rich telluride component, moncheite and kotulskite are joined by a third telluride phase with a composition close to Pd_3Te_2, forming up to 30 μm sized, bright yellowish euhedral grains inside iss. No telluride with that composition has yet been reported from natural assemblages.

In order to verify that equilibrium was reached with our experimental technique (i.e. controlled cooling from superliquidus temperature to run temperature), the 400 and 500°C experiments were reversed. Reversals were achieved by melting both charges at 1,150°C, quenching them in air to room temperature in about 30 s, and only then heating up the quenched charges to their designated run temperatures (400, 500°C). Both reversals gave the same phase compositions as their continuously cooled equivalents and so we have little doubt that chemical equilibrium was reached. Texturally, however, the reversals were quite different in that they preserved rather well dendritic mss quench crystals inherited from the initial quenching phase, which the slowly cooled equivalents did not do.

Phase chemistry

All equilibrium phases were analyzed with a JEOL electron microanalyser at 20 kV and 15 nA. Base metals and S were analyzed on K_α, Pd and Te on L_α, and Pt on M_α. Cu, Fe, Ni, and S were calibrated on natural sulfides, and Pt, Pd, and Te on the pure metals. Most phases were analyzed in spot mode; but some phases, notably exsolved mss, were analyzed with a beam defocused to 50 μm. Counting times were 30 s on peak and background. Detection limits for Pd, Pt and Te are ~500 ppm. Phase compositions are summarized in Tables 3 and 4.

Monosulfide solid solution (mss)

Compositional trends of the monosulfides are illustrated in Fig. 3. Ni increases with falling temperature, from ~10 at the liquidus to >22 wt%, before mss breaks down to pyrrhotite and pentlandite. In the charges with the Te-rich telluride component, Ni in mss tends to be slightly lower at least in the high temperature runs, which is surprising considering that the Te-rich telluride component contained Ni in addition to Pd and Pt. Apparently, Te in a sulfide system influences the partitioning behavior of Ni by stabilizing Ni in the melt. Cu in mss passes through a maximum with falling temperature, from 2.5 wt% at 1,015°C to >4 wt% at 825°C, then dropping to 0.25 wt% in the lowest temperature run. The Cu maximum is more pronounced in the experiments with the metal-rich telluride component for which we have a better temperature coverage. It coincides texturally with the solidus of the sulfide melt.

Significant differences between the two telluride-bulk compositions are noted with respect to Pd and Pt. In experiments with the Te-poor telluride component, Pt is detectable in mss only above 920°C, to drop rapidly to <500 ppm in all experiments below 825°C. Pd shows a temperature dependence identical to that of Cu, first a steady increase with falling temperature to a maximum of 0.4 wt% at ~625°C, followed by a decrease to below detection limit at 370°C. The Pd maximum is shifted relative to the Cu maximum to lower temperature, by about 100°C. It coincides with the solidus of the Pd-rich telluride melt, which we place based on textural considerations (i.e., first appearance of euhedral kotulskite) at >625°C. In contrast, in the

Table 3 Phase compositions (in wt%) of experiments with the Te-rich telluride component

Run number	HH40	HH21	HH27	HH28	HH26	HH42
Temperature (°C)	900	700	600	500	400	320
Monosulfide solid solution (mss)						
No. of analyses	8	9	8	7	4	6
Fe	50.0 ± 0.75	40.7 ± 0.33	39.9 ± 0.47	40.6 ± 0.22	39.6 ± 0.27	30.6 ± 0.71
Ni	10.3 ± 0.75	18.1 ± 0.76	19.4 ± 0.28	20.0 ± 0.25	22.1 ± 0.12	31.8 ± 0.71
Cu	2.65 ± 0.26	2.97 ± 0.53	1.76 ± 0.05	0.87 ± 0.03	0.41 ± 0.03	0.17 ± 0.08
Pd	ND	ND	ND	ND	ND	ND
Pt	ND	ND	ND	ND	ND	ND
Te	0.31 ± 0.02	0.29 ± 0.04	0.31 ± 0.04	0.29 ± 0.03	0.26 ± 0.04	0.39 ± 0.11
S	36.6 ± 0.25	37.6 ± 0.29	37.7 ± 0.24	37.1 ± 0.50	37.7 ± 0.20	36.6 ± 0.19
Atomic metal/S	0.97 ± 0.03	0.92 ± 0.03	0.91 ± 0.02	0.93 ± 0.02	0.93 ± 0.01	0.96 ± 0.03
Intermediate solid solution (iss)						
No. of analyses		4	5	5	2	6 (pent)
Fe	iss	35.4 ± 0.13	36.6 ± 0.17	37.8 ± 0.90	38.8 ± 0.09	26.4 ± 0.22
Ni	Unstable	4.61 ± 0.04	4.36 ± 0.08	4.47 ± 0.03	4.03 ± 0.08	40.3 ± 0.10
Cu		24.7 ± 0.19	23.1 ± 0.30	21.1 ± 0.08	21.2 ± 0.01	0.48 ± 0.06
Pd		ND	0.05 ± 0.04	0.07 ± 0.05	0.07 ± 0.01	0.06 ± 0.07
Pt		ND	ND	ND	ND	ND
Te		0.23 ± 0.02	0.36 ± 0.06	0.44 ± 0.08	0.36 ± 0.02	0.46 ± 0.06
S		34.6 ± 0.17	34.8 ± 0.20	34.3 ± 0.68	35.1 ± 0.20	32.4 ± 0.12
Atomic metal/S		1.02 ± 0.01	1.00 ± 0.01	1.01 ± 0.04	1.00 ± 0.01	1.15 ± 0.01
Moncheite solid solution						
No. of analyses	7	15	5	3	3	6
Fe	0.13 ± 0.16	0.48 ± 0.68	0.36 ± 0.37	0.09 ± 0.11	0.26 ± 0.17	0.07 ± 0.07
Ni	0.72 ± 0.06	4.71 ± 0.95	1.51 ± 0.33	1.56 ± 0.13	1.61 ± 0.16	1.76 ± 0.34
Cu	0.04 ± 0.03	0.34 ± 0.45	0.13 ± 0.10	0.10 ± 0.07	0.16 ± 0.11	0.02 ± 0.02
Pd	1.04 ± 0.09	8.21 ± 1.60	2.07 ± 0.22	2.68 ± 0.26	2.53 ± 0.17	1.50 ± 0.27
Pt	38.8 ± 0.25	19.6 ± 4.10	35.9 ± 0.97	34.7 ± 1.16	34.8 ± 0.59	36.2 ± 0.87
Te	58.0 ± 0.38	66.5 ± 2.21	59.6 ± 0.35	59.7 ± 0.16	59.7 ± 0.41	59.9 ± 0.44
Atomic metal/Te	0.49 ± 0.01	0.50 ± 0.07	0.51 ± 0.02	0.50 ± 0.02	0.51 ± 0.01	0.49 ± 0.02
Pd–Te phases						
No. of analyses	4 (melt)	4 (melt)	9 (mer)	8 (mer)	7 (mer)	6 (mer)
Fe	2.13 ± 1.83	0.19 ± 0.07	0.42 ± 0.23	0.34 ± 0.24	0.31 ± 0.21	0.15 ± 0.09
Ni	13.5 ± 7.99	4.84 ± 0.34	9.19 ± 0.48	8.95 ± 1.02	9.45 ± 0.57	6.12 ± 0.35
Cu	1.97 ± 1.11	0.15 ± 0.06	0.34 ± 0.19	0.34 ± 0.32	0.24 ± 0.13	0.05 ± 0.05
Pd	13.4 ± 3.34	18.6 ± 1.72	15.8 ± 0.76	14.3 ± 0.96	15.5 ± 0.74	19.2 ± 0.60
Pt	8.37 ± 6.10	8.74 ± 0.72	1.08 ± 1.40	3.45 ± 2.51	0.59 ± 0.66	1.1 ± 0.14
Te	58.7 ± 3.39	66.4 ± 0.98	74.3 ± 0.43	71.8 ± 1.03	73.9 ± 1.25	74.4 ± 0.32
Atomic metal/Te	1.02 ± 0.19	0.59 ± 0.03	0.56 ± 0.02	0.56 ± 0.04	0.55 ± 0.02	0.50 ± 0.01

Average compositions, ± ranges are 1 sigma standard deviations, *ND* not detected. Abbreviations as in Table 2

Te-rich charges mss is nearly Pd–Pt free at all temperatures. The higher Te/S bulk ratio of these charges apparently stabilized Pd and Pt as Pd–Te and Pt–Te complexes in the melt, preventing precious metals to partition significantly into mss.

Te concentration in mss depends slightly on Te/S bulk ratio. With the Te-rich telluride component, mss reaches 0.3 ± 0.05 wt% Te, whereas in the metal-rich charges mss only incorporates 0.2 wt% Te. Interestingly, in both sets of experiments Te in mss is nearly independent of temperature, indicating that Te partitions into mss as an anion replacing S. The lack of temperature dependence has consequences for the crystallization temperature of tellurides in natural sulfide ores, to be discussed below.

Intermediate solid solution (iss)

In iss, Cu falls with falling temperature, in both the metal-rich and Te-rich charges by about the same extent (Fig. 4). Ni shows a very minor decrease from ~5 in the highest temperature iss, to <3.5 wt% in the lowest temperature iss. Both Cu and Ni are balanced by a complementary increase in Fe. Since Ni and Cu also fall in mss (Fig. 3), modal iss must increase in the charges as temperature falls; above the sulfide solidus at the expense of residual sulfide melt and below the solidus by volume exsolution of Cu–Ni components from mss. For Te, we note no clear trend except that in runs with the Te-rich telluride component, iss is generally richer in Te. Overall, Te concentrations are

Table 4 Phase compositions (in wt%) of experiments with the metal-rich telluride component

Run number	HH3	HH4	HH2	HH6	HH1	HH10	HH11
Temperature (°C)	1015	920	825	725	625	500	370
Monosulfide solid solution (mss)							
No. of analyses	5	5	5	7	6	9	9
Fe	48.3 ± 0.37	44.1 ± 0.22	41.6 ± 0.29	41.2 ± 0.54	40.4 ± 0.36	40.2 ± 0.19	39.8 ± 0.12
Ni	10.5 ± 0.13	14.3 ± 0.12	16.7 ± 0.89	17.4 ± 0.34	18.5 ± 0.17	20.3 ± 0.14	21.2 ± 0.22
Cu	2.49 ± 0.17	3.91 ± 0.05	4.50 ± 0.60	3.16 ± 0.62	2.28 ± 0.06	1.16 ± 0.12	0.26 ± 0.06
Pd	0.19 ± 0.05	0.29 ± 0.04	0.32 ± 0.09	0.33 ± 0.10	0.43 ± 0.05	0.21 ± 0.05	0.03 ± 0.05
Pt	0.29 ± 0.06	0.22 ± 0.04	ND	ND	0.05 ± 0.04	ND	0.05 ± 0.04
Te	0.21 ± 0.02	0.24 ± 0.03	0.20 ± 0.05	0.17 ± 0.06	0.21 ± 0.02	0.20 ± 0.03	0.20 ± 0.02
S	38.3 ± 0.20	38.2 ± 0.07	37.7 ± 0.47	37.6 ± 0.33	37.7 ± 0.22	38.1 ± 0.24	38.2 ± 0.28
Atomic metal/S	0.91 ± 0.01	0.92 ± 0.01	0.94 ± 0.04	0.92 ± 0.03	0.92 ± 0.01	0.91 ± 0.01	0.91 ± 0.01
Intermediate solid solution (iss)							
No. of analyses			5	6	7	8	6
Fe			32.1 ± 0.72	34.1 ± 0.44	36.4 ± 0.39	38.4 ± 0.37	38.4 ± 0.14
Ni			4.97 ± 0.24	4.70 ± 0.08	4.15 ± 0.20	3.86 ± 0.05	3.20 ± 0.07
Cu			29.3 ± 1.00	26.6 ± 0.54	23.6 ± 0.43	22.2 ± 0.24	21.9 ± 0.32
Pd			ND	ND	0.05 ± 0.06	0.06 ± 0.02	ND
Pt			ND	ND	ND	ND	ND
Te			0.17 ± 0.05	0.07 ± 0.02	0.06 ± 0.05	0.09 ± 0.03	0.08 ± 0.02
S			33.7 ± 0.31	34.4 ± 0.20	34.6 ± 0.22	35.4 ± 0.29	35.8 ± 0.10
Atomic metal/S			1.06 ± 0.04	1.03 ± 0.02	1.01 ± 0.02	1.00 ± 0.02	0.97 ± 0.01
Moncheite solid solution							
No. of analyses		6	10	10	8	4	2
Fe		0.07 ± 0.05	0.26 ± 0.22	0.29 ± 0.23	0.23 ± 0.19	0.17 ± 0.16	0.22 ± 0.02
Ni		0.23 ± 0.02	0.35 ± 0.24	0.34 ± 0.21	0.14 ± 0.09	0.09 ± 0.09	0.04 ± 0.00
Cu		0.08 ± 0.04	0.15 ± 0.15	0.16 ± 0.12	0.07 ± 0.04	0.06 ± 0.09	0.29 ± 0.09
Pd		1.89 ± 0.06	3.34 ± 0.08	3.93 ± 0.10	3.02 ± 0.16	1.54 ± 0.47	2.73 ± 0.10
Pt		39.3 ± 0.25	37.0 ± 0.46	36.1 ± 0.37	37.9 ± 0.23	39.9 ± 0.55	38.1 ± 0.14
Te		58.0 ± 0.36	58.3 ± 0.24	58.8 ± 0.24	57.7 ± 0.17	57.2 ± 0.22	57.8 ± 0.11
Atomic metal/Te		0.50 ± 0.01	0.51 ± 0.01	0.51 ± 0.01	0.51 ± 0.01	0.50 ± 0.01	0.51 ± 0.00
Pd–Te phases							
No. of analyses		4 (melt)	7 (melt)	9 (melt)	10 (kot)	7 (kot)	5 (kot)
Fe		0 ± 0.02	0.28 ± 0.15	0.58 ± 0.35	0.38 ± 0.26	0.28 ± 0.30	0.33 ± 0.16
Ni		1.2 ± 0.02	0.75 ± 0.08	0.53 ± 0.22	0.28 ± 0.07	0.11 ± 0.02	0.10 ± 0.02
Cu		0.4 ± 0.05	0.45 ± 0.74	0.39 ± 0.18	0.38 ± 0.14	0.21 ± 0.21	0.24 ± 0.17
Pd		39 ± 0.19	41.8 ± 1.62	41.5 ± 0.72	40.5 ± 0.79	43.0 ± 0.44	43.4 ± 0.44
Pt		1.9 ± 0.07	2.6 ± 0.35	2.9 ± 0.26	2.72 ± 0.11	1.50 ± 0.10	0.60 ± 0.15
Te		57 ± 0.22	54.6 ± 1.15	54.5 ± 0.52	55.1 ± 0.56	55.3 ± 0.12	54.9 ± 0.28
Atomic metal/Te		0.90 ± 0.02	1.01 ± 0.02	1.01 ± 0.02	0.95 ± 0.02	0.97 ± 0.01	0.98 ± 0.01

Average compositions, ± ranges are 1 sigma standard deviations, *ND* not detected. Abbreviations as in Table 2

similar to Te in mss. Both Pt and Pd are below electron probe detection limit.

Tellurides

Experimental telluride compositions are illustrated in Fig. 5. We combine Pd and Ni in one component, to be able to discriminate between phase compositions with different metal/Te ratios and display phases like moncheite, merenskyite, and kotulskite in one diagram. In both bulk compositions, moncheite is the high temperature telluride, coexisting either with telluride melt, merenskyite or kotulskite. Moncheite shows little systematic compositional variation and is strictly stoichiometric. Only in the 700°C do we note unusually high Ni and Pd contents, perhaps coinciding with maxima in the $PdTe_2$ and $NiTe_2$ activities in the coexisting, near-solidus telluride melt. Merenskyite and kotulskite, in contrast, are not perfectly stoichiometric (Kim and Chao 1991), and the M/Te ratios of both phases are slightly temperature dependent (Fig. 6). Like in the natural assemblages, if there is solid solution, it is limited to the Pd endmember compositions because a kotulskite equivalent with the composition PtTe does not seem to exist in nature. The extent of MTe–MTe_2 solid solution is less than in nature (cf. Fig. 1c) but note that the two phases (mer and kot) in Fig. 6 were not found coexisting with each

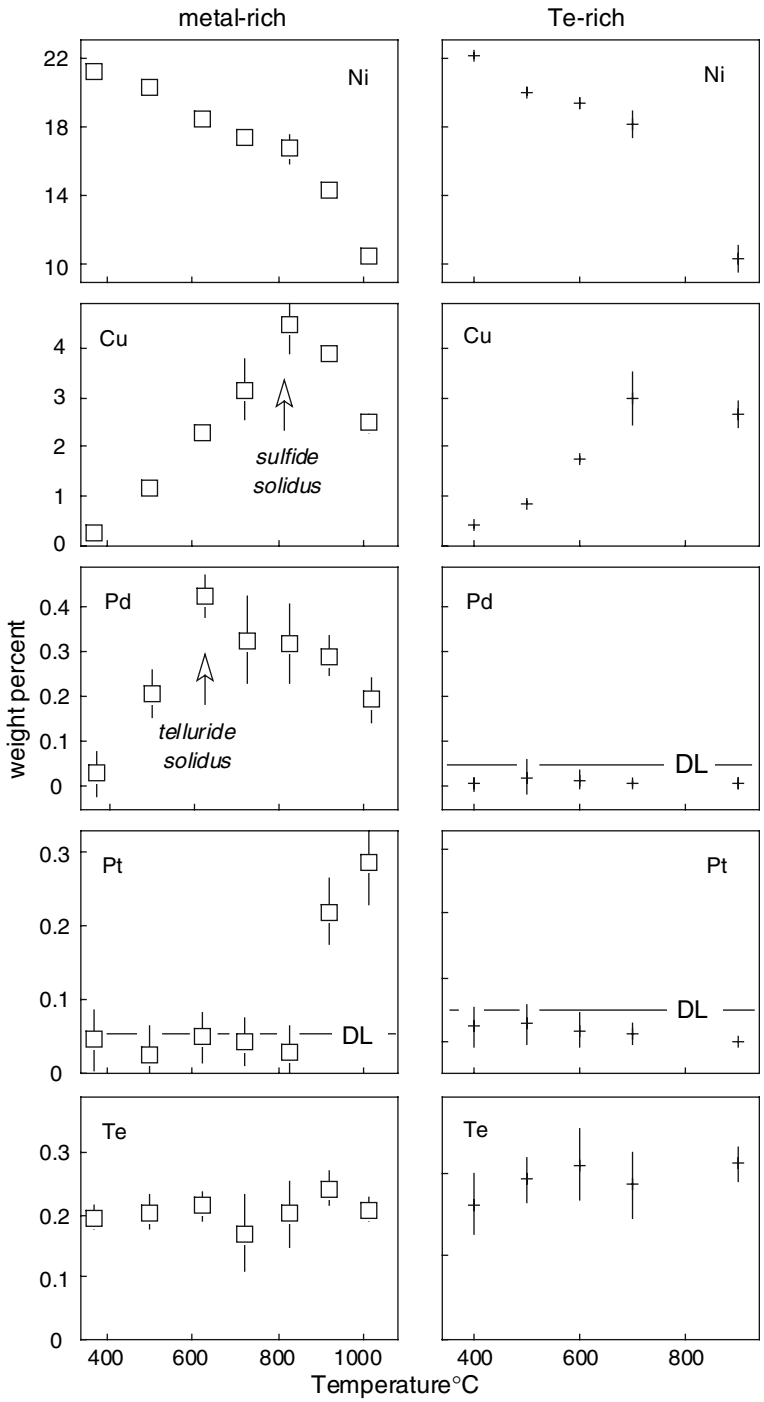

Fig. 3 Monosulfide (*mss*) compositions from metal-rich and Te-rich telluride experiments. Mss compositions from the 320°C run (HH42) are not included because that run had a different bulk composition. *DL* detection limit

other, so their metal/Te ratios do not necessarily outline a solvus. In addition, many natural tellurides contain Bi and Sb in addition to Te, which may promote solid solution between MTe and MTe_2 stoichiometries.

In none of the experimental charges, Ni-dominated (Ni,Pd,Pt)Te_2 phase compositions were observed, not even in the 320°C experiment HH42 to which we added extra Ni to stabilize melonite.

Sulfide and telluride melts

Sulfide melt compositions were not analyzed systematically because equilibrium compositions are so difficult to quench. Relative to the solid sulfides, the sulfide melt is enriched in Cu and Ni as expected from the mss–sulfide melt partition coefficients (Ballhaus et al. 2001). Te contents in the quench products of sulfide melt are in the sub-percentage range, and S content in

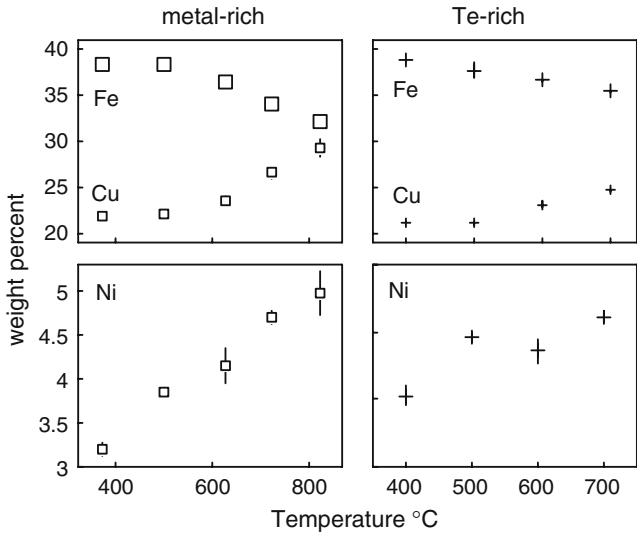

Fig. 4 Compositions of intermediate solid solutions (*iss*) from metal-rich and Te-rich telluride experiments against experimental run temperatures. Iss from HH42 not included because of different bulk composition

quenched telluride melt is near detection limit, apparently supporting the conclusion based on texture (cf. Fig. 2f, g) that sulfide and telluride melts are poorly miscible. However, whether these concentrations are actual solubilities is largely subject to interpretation; if we interpreted all telluride patches in the quench products of sulfide melt as being quench precipitates, i.e. a telluride component originally dissolved in sulfide melt but precipitated when the sulfide quench-crystallized, the actual solubility of Te in sulfide melt would be considerably higher.

Discussion

The experiments were motivated by the question whether or not sulfide–silicate textures provide any quantitative temperature information on the mode of mineralization. For sulfide–telluride styles of mineralization, this is clearly not the case. Neither the presence nor the extent of a hydrothermal overprint, evident by hydrous sulfide and silicate alteration, can be cited as evidence that Te or the precious metals were added via hydrothermal fluids. Our experimentally determined crystallization sequences illustrate how tellurides may become enriched in evolving sulfide systems. Phase compositions and phase assemblages place the equilibrium temperatures of natural sulfide–telluride assemblages in the low temperature realm, possibly at below 200–300°C. This conclusion is valid, regardless of the degree of hydrothermal overprint evident in the ore textures.

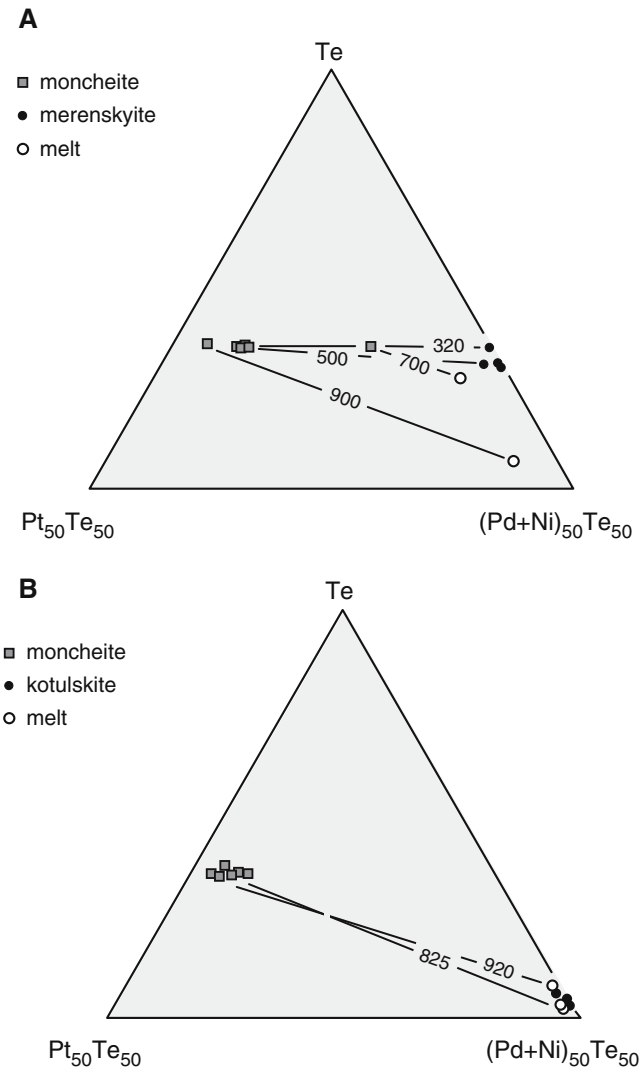

Fig. 5 Average experimental telluride compositions of all experiments in the Pt – (Pd + Ni) – Te ternary diagram (cf. Tables 3, 4). **a** Moncheite–merenskyite assemblages in experiments with the Te-rich telluride component, and **b** Moncheite–kotulskite in experiments with the metal-rich telluride component. Some coexisting phases connected by *tie lines*, labelled with run temperature

Crystallization sequence in the experiments

In the experimental charges, monosulfide is the first phase to crystallize. Mss fractionation will enrich the sulfide melt in Te as well as Pt and Pd, the latter according to the mss–sulfide melt partition coefficients (Li et al. 1996; Ballhaus et al. 2001). It is critical to emphasize how strongly Pt and Pd are complexed by telluride. Even a modest increase in bulk Te relative to Pt and Pd (cf. Table 1) rendered magmatic mss and iss practically PGE-free. Apparently, Pt and Pd can only be substituted in base metal sulfide phases if they are

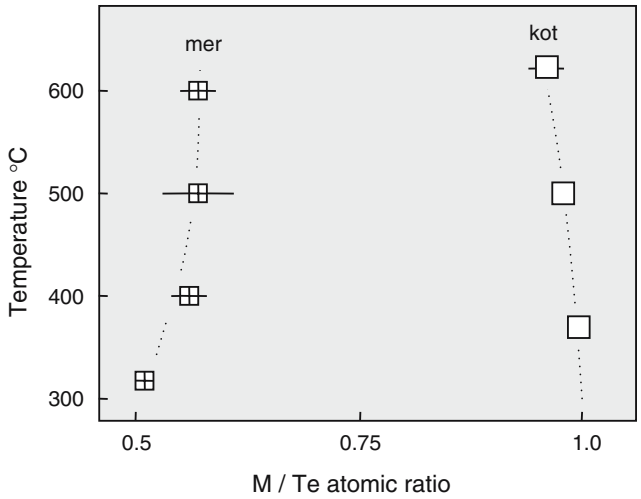

Fig. 6 Metal/Te atomic ratios of the experimental Pd-rich telluride compositions merenskyite (mer; *crossed squares*) and kotulskite (kot; *open squares*) against run temperature. Whether or not the two phases outline solvus flanks remains unclear, as none of the experimental charges returned coexisting merenskyite–kotulskite assemblages. Note that in all runs shown the phase buffering MTe_2 stoichiometry is moncheite which is poorly miscible with PdTe (Fig. 1c), and therefore actual miscibility along the PdTe–$PdTe_2$ binary join is likely to be higher than implied by this diagram (cf. Hoffman and McClean 1976). The telluride solidus is >625°C. *Error bars* are cumulative one sigma errors calculated from analytical ranges

present in the equilibrium sulfide melt as ions or as sulfide complexes. However, if they are complexed to Te, they remain in the melt. Hence, the effect of Te (and presumably of As, Bi, and Sb) in a fractionating sulfide melt is to lower the already low mss–sulfide melt Pt–Pd partition coefficients (<0.1) even further (Fleet et al. 1993). Arsenic appears to have a similarly strong affinity to complex with Pt, Pd, and Rh; wherever arsenide phases are present in sulfide, the sulfide phases tend to be impoverished in these elements (Gervilla et al. 1996, 1998; Holwell and McDonald 2006).

In the experiments, falling temperature and protracted mss fractionation caused a shift in bulk melt composition to higher Te/S bulk ratios, until a separate telluride melt is exsolved. Based on textures and the temperature dependent Cu–Pd concentrations in mss (Fig. 3), it is possible that two melt phases coexisted between 1,015 and 825°C, a Cu–Ni-enriched sulfide melt and a Pd–Ni-rich telluride melt. In the experiment at 920°C (Fig. 2g), little doubt remains that sulfide and telluride constitute an immiscible system. Perhaps we can go as far as stating that the crystallization of moncheite requires the presence of a separate telluride melt, because in all charges where moncheite is stable, moncheite needles are either wetted by Pd–Ni-enriched telluride melt or are intergrown with merenskyite or kotulskite. If moncheite was able to crystallize directly from a moncheite-saturated sulfide melt, we should occasionally encounter moncheite inclusions in mss without attached or intergrown Pd–Ni telluride phases, but this was never observed in the experiments. Note though that in nature, isolated moncheite laths included in pyrrhotite and pentlandite do of course occur quite frequently (e.g. Ballhaus and Stumpfl 1986; Oberthür et al. 2003) but natural sulfides are less rigorous in preserving original magmatic textures than short-lived, rapidly quenched experiments, and therefore less informative about processes.

Once iss is a stable phase, the sulfide solidus is reached rather quickly, because iss has a composition close to that of the final Cu–Ni ± Fe–S sulfide melt. The sulfide solidus occurs in both compositions at about the same temperature, i.e. between 820 and 850°C. It is unaffected by bulk (Pt + Pd)/Te, corroborating our notion based on texture that the solubility of Te in sulfide melt is rather insignificant. Of all major elements in mss–sulfide melt systems, Cu is one of the most incompatible ($D_{Cu}^{mss-sulfide\ melt} \sim 0.2$; Ballhaus et al. 2001), and therefore the sulfide solidus can be correlated with a maximum in Cu in solid solution in mss (cf. Fig. 3).

The telluride solidus occurs at a lower temperature than the sulfide solidus. It depends strongly on the PGE/Te ratio of the telluride melt. In bulk compositions where the atomic (Pt + Pd)/Te is so high that not all PGE can be complexed with Te, which is the case for our metal-rich bulk composition, the telluride solidus is marked by a distinct maximum in Pd in solid solution in mss, i.e. around 625°C (Fig. 3).

Application to nature

Natural sulfide–telluride systems contrast with our experimental compositions in that natural sulfide melts must have much less Te and lower Te/S bulk weight ratios. Our highest temperature monosulfides have Te/S weight ratios around 9×10^{-3}. Not much is known about Te concentrations in natural magmatic sulfide melts; however, the Te/S ratio is likely to be much lower. Because Te is chalcophile we may assume that natural bulk sulfide Te/S weight ratios are similar to Te/S ratios of CI chondrite and primitive mantle ($\sim 4 \times 10^{-5}$; Palme and O'Neill 2003). For primitive basaltic melts we calculate a Te/S weight ratio of $\sim 2 \times 10^{-5}$ (Hertogen et al. 1980; Yi et al. 2000) assuming the basalts analyzed by these authors contained 1,000 ppm dissolved S (O'Neill and Mavrogenes

2002). Piña et al. (2006) report (Te + Bi)/S weight ratios for bulk Fe–Ni–Cu sulfides from the Aguablanca Ni–Cu deposit of ~2.7×10^{-5} which is fairly close to the calculated basaltic ratio. The effect of a bulk Te/S ratio lower than in natural sulfide melts is to shift telluride saturation to lower temperatures than in our experiments, very probably extremely close to the sulfide solidus (cf. Cabri and Laflamme 1976).

Natural sulfide melts also have lower (Pt + Pd)/semimetal ratios than any of the charges used here. For the primitive tholeiite compositions of Hertogen et al. (1980), we calculate a (Pt + Pd)/(Te + Sb + Bi) weight ratio of ~0.3. Note that Pt was not analyzed by Hertogen et al. (1980), so Pt concentrations in their most primitive basalts are estimated to around 5.5 ppb, i.e. slightly below a primitive mantle concentration, which is a reasonable Pt concentration for a primitive tholeiitic basalt. Piña et al. (2006) report (Pt + Pd)/(Te + Sb + Bi) weight ratios for massive magmatic sulfide of ~0.2–0.3. All these natural ratios are lower than in our experiments. Given that Pt and Pd form highly stable complexes with semi-metals, the effect of a low (Pt + Pd)/(Te + Sb + Bi) bulk ratio is to prevent Pt and Pd from substituting in sulfide phases, i.e. keep them as long as possible dissolved in the sulfide melt until a discrete bismuthotelluride melt can exsolve.

Equilibration temperatures of natural sulfide–telluride assemblages

Finally, we discuss whether the distinction based on texture between magmatic and hydrothermal phase assemblages is also reflected in phase compositions and phases assemblages. Te concentrations in mss and iss can be utilized as a semiquantitative thermometer to broadly constrain equilibration temperatures of natural sulfide–telluride assemblages. In our experimental mss and iss, Te constantly ranges around 0.2–0.3 wt%. We note no temperature dependence or affinity of Te to a certain sulfide crystal structure. Even in the lowest temperature experiment (320°C), Te in mss still is at the same concentration level as in the highest temperature mss. Presumably this is so because Te in sulfide lattices replaces S, hence is unaffected by temperature sensitive order–disorder reactions in the metal sublattice of the sulfide phase (cf. Ballhaus and Ulmer 1995). In natural sulfides, Te concentrations appear to be much lower. Hattori et al. (2002) analyzed Te in mantle sulfides with PIXE to ~100 ppm. We tried to verify these concentrations by analyzing with laser-ablation ICP-MS natural pentlandites from the Merensky reef that coexist with various PGE phases including bismuthotellurides. In contrast to Hattori et al. (2002), we find no Te concentrations above the Te detection limit of the laser probe (conservatively estimated to be around 1 ppm). Obviously, natural sulfides are more extensively reset than our lowest temperature experiment (320°C). During resetting, Te exsolves, presumably as $NiTe_2$ and/or as $PdTe_2$ components (see below). It is likely that Te exsolution coincides with the recrystallization of mss and iss to monoclinic pyrrhotite, pentlandite, and chalcopyrite.

The natural Pt–Pd bismuthotelluride compositions compiled in Fig. 1 probably do not give meaningful temperature information. For example, in nature, merenskyite–melonite solid solutions are near complete (Fig. 1b), whereas our synthetic merenskyites have more restricted Pd/Ni atomic ratios ranging from 0.6 to 1.1 (Table 3). Natural Pt–Pd tellurides also are more flexible with respect to the Pt/(Pd + Ni) atomic ratio than our experimental moncheites, most of which are close to endmember $PtTe_2$ composition (cf. Fig. 6). Perhaps in nature, solid solution is aided by the presence of Bi and Sb, elements that we did not include in our study, but it is also possible that natural tellurides are modified by low-temperature Te exsolution from sulfides. Any Te that exsolves when high-temperature mss and iss are replaced by pyrrhotite, pentlandite, chalcopyrite and pyrite, will either crystallize as discrete melonite $(\underline{Ni},Pt,Pd)(\underline{Te},Sb,Bi)_2$ or will precipitate on the surfaces of earlier, higher temperature Pt–Pd telluride phases, potentially overprinting former equilibrium compositions and producing at least part of the scatter displayed by Fig. 1b. Therefore, caution is advised when using natural telluride compositions as quantitative thermometers (cf. Hoffman and MacLean 1976; Piña et al. 2006).

Late Te exsolution from sulfide may also be the reason why no experiment returned true melonite $NiTe_2$ compositions, not even the Ni-enriched, lowest temperature experiment HH42 (320°C). Principally, melonite should be expected to form only when after crystallization of the precious metal (Pt–Pd–Au–Ag) tellurides, there is still sufficient Te in the system to stabilize intermetallic compounds with less precious elements, like $NiTe_2$. In natural sulfide melts (cf. Fig. 1a) this is likely to be the case; bulk atomic (Pt + Pd + Au + Ag)/semimetal ratios of natural sulfide melts are probably around 0.2–0.3, i.e. lower than the MTe_2 stoichiometry of the most Te-rich telluride phases and lower than in our charges. On the other hand, many natural melonites may be subsolidus exsolution products, crystallizing when mss and iss are replaced by a low-temperature pyrrhotite–pentlandite–chalcopyrite–pyrite assemblage, i.e. when Te in solid solution in sulfide is expelled. None of our experiments

reached the temperature range (~200°C) where this is likely to happen (cf. Ballhaus and Ulmer 1995), and therefore it should not come as a surprise that we could not stabilize Ni-rich tellurides.

Conclusions

1. Sulfide and telluride melts constitute an immiscible system. When Te–Bi–Sb-bearing sulfide melt fractionates, a discrete bismuthotelluride melt will exsolve shortly before the sulfide solidus is reached, scavenging Pt and Pd originally contained in the sulfide melt. The timing of telluride exsolution is controlled by the Te/S and (Pt + Pd)/semimetal bulk ratios. Our results support Cabri and Laflamme's (1976) model by which polyphase precious metal telluride assemblages in sulfide ore (cf. Helmy 2004) may originally have been droplets of an immiscible bismuthotelluride liquid that exsolved from a late-stage, highly fractionated, Cu-enriched sulfide melt.
2. Pt–Pd-dominated tellurides as they occur in Pt–Pd-rich sulfide deposits like the Merensky reef and the Platreef cannot form easily by solid-state exsolution from sulfides, unlike PGE sulfides (Ballhaus and Ulmer 1995). Semimetals like Te, Sb, and Bi are such potent complexing agents for Pt and Pd that in their presence, no Pt and little Pd will enter the lattices of high-temperature sulfides. Hence, upon cooling, no Pt and little Pd can exsolve from reequilibrating sulfide phases. The only telluride phase that may form by exsolution from base metal sulfides is melonite. It is anticipated that arsenic will have a similarly strong effect on PGE partitioning, since As forms stable high-temperature phases with Pt and Rh, including sperrylite ($PtAs_2$), hollingworthite (Rh,Pt,Pd)AsS, and platarsite (Pt,Rh,Ru)AsS.
3. The composition of telluride phases can serve as a qualitative indicator for the PGE potential of a magmatic sulfide deposit. If Ni-rich tellurides occur in abundance (cf. Fig. 1a), both the (Pt + Pd)/semimetal bulk ratio and the absolute Pt and Pd concentrations in the sulfide melt are likely to have been low at the time of telluride crystallization, and consequently, the potential of that sulfide deposit for extensive Pt–Pd mineralization will also be low. If, on the other hand, Ni-poor Pt–Pd tellurides prevail, such as in the classic PGE-rich sulfide deposits of the Bushveld and Great Dyke complexes, the sulfide ore is potentially PGE-rich.
4. The distinction based on ore texture between magmatic and hydrothermal sulfide–telluride ore should only be made in descriptive terms. It carries no meaningful temperature information. Based on Te solubility in $(Fe,Ni,Cu)_{1-x}S$ monosulfide (~0.2–0.3 wt%), all styles of sulfide–telluride mineralizations reported in the literature are reset to temperatures well below 320°C, our lowest experimental temperature. These temperatures are closure temperatures. They relate in no way to the origin of the PGE mineralization or the mode of PGE enrichment.

Acknowledgments This work was financed generously by a DFG scholarship to Hassan Helmy and by the DFG grants BA 964/23-1 and 24-1 to Chris Ballhaus. The polished sections were prepared by Paul Löbke. Claudia Meyer is thanked for logistic help during Hassan Helmy's sabbatical in Münster. David Holwell, Thomas Oberthür, and Frank Melcher kindly provided unpublished telluride phase compositions from the Platreef (northern Bushveld Complex), the Hartley mine (Great Dyke), and the Driekop pipe (Bushveld Complex), respectively. Comments by Giorgio Garuti and an anonymous reviewer greatly improved the paper.

References

Ballhaus C, Stumpfl EF (1986) Sulfide and platinum mineralization in the Merensky reef: evidence from hydrous silicates and fluid inclusions. Contrib Mineral Petrol 94:193–204

Ballhaus C, Ryan CG (1995) Platinum-group elements in the Merensky reef. I. PGE in solid solution in base metal sulfides and the down-temperature equilibration history of Merensky ores. Contrib Mineral Petrol 122:241–251

Ballhaus C, Ulmer P (1995) Platinum-group elements in the Merensky reef. II. Experimental solubility of Pt and Pd in synthetic $Fe_{1-x}S$ between 950 and 450° under controlled f_{S2} and f_{H2}. Geochim Cosmochim Acta 59:4881–4888

Ballhaus C, Tredoux M, Spaeth A (2001) Phase relations in the Fe–Ni–Cu–PGE–S system at magmatic temperature and application to massive sulphide ores of the Sudbury igneous complex. J Petrol 10:1911–1926

Barkov AY, Laflamme JHG, Cabri LJ, Martin RF (2002) Platinum-group minerals from the Welgreen Ni–Cu–PGE deposit, Yukon, Canada. Can Mineral 40:651–669

Barkov A, Thibault Y, Laajoki KVO, Melezhik VA, Nilsson LP (1999) Zoning and substitutions in Co–Ni–(Fe)–PGE sulfarsenides from the Mount General Skya layered intrusion, Arctic Russia. Can Mineral 37:127–142

Cabri LJ, Laflamme JHG (1976) The mineralogy of the platinum-group elements from some copper–nickel deposits of the Sudbury area, Ontario. Econ Geol 71:1159–1195

Cawthorn RG, Lee CA, Schouwstra RP, Mellowship P (2002) Relationship between PGE and PGM in the Bushveld Complex. Can Mineral 40:311–328

Craig JR (1973) Pyrite–pentlandite and other low temperature assemblages in the Fe–Ni–S system. Am J Sci 273:496–510

Etschmann B, Pring A, Putnis A, Grguric BA, Studer A (2004) A kinetic study of the exsolution of pentlandite $(Ni,Fe)_9S_8$ from the monosulfide solid solution (Fe,Ni)S. Am Mineral 89:39–50

Farrow CFG, Watkinson DH (1992) Alteration and the role of fluids in Ni, Cu, and platinum-group element deposition, Sudbury Igneous Complex Contact, Onaping-Levack area, Ontario. Mineral Petrol 46:67–83

Fleet ME, Chryssoulis SL, Stone WE, Weisener CG (1993) Partitioning of the platinum-group elements in the Fe–Ni–Cu–S system: experiments on the fractional crystallization of sulfide melt. Contrib Mineral Petrol 115:36–44

Garuti G, Rinaldi R (1986) Mineralogy of melonite-group and other tellurides from the Ivrea–Verbano basic complex, western Italian Alps. Econ Geol 81:1213–1217

Gervilla F, Kojonen K (2002) The platinum-group minerals in the upper section of the Keivitsansarvi Ni–Cu–PGE deposit, northern Finland. Can Mineral 40:377–394

Gervilla F, Sanchez-Anguita A, Acevedo RD, Fenoll Hach-Ali P, Paniagua A (1997) Platinum-group element sulpharsenides and Pd bismuthotellurides in the metamorphosed Ni–Cu deposit at Las Aguilas (Province of San Luis, Argentina). Min Mag 61:861–877

Gervilla F, Leblanc M, Torres Ruiz J, Hachali PF (1996) Immiscibility between arsenide and sulfide melts: a mechanism for the concentration of noble metals. Can Mineral 34:485–502

Gervilla F, Papunen H, Kojonen K, Johanson B (1998) Platinum, palladium, and gold-rich arsenide ores from the Kylmakoski Ni–Cu deposit (Vammala Nickel Belt, SW Finland). Mineral Petrol 64:163–185

Hattori KH, Arai S, Clarke DB (2002) Selenium, tellurium, arsenic and antimony contents of primary mantle sulfides. Can Mineral 40:637–650

Helmy HM (2004) Cu–Ni–PGE mineralization in the Genina Gharbia mafic–ultramafic intrusion, Eastern Desert, Egypt. Can Mineral 42:351–370

Helmy HM (2005) Melonite-group minerals and other tellurides from three Cu–Ni–PGE prospects, Eastern Desert, Egypt. Ore Geol Rev 26:305–324

Helmy HM, Mogessie A (2001) Gabbro Akarem, Eastern Desert, Egypt: Cu–Ni–PGE mineralization in a concentrically zoned mafic–ultramafic complex. Mineral Depos 36:58–71

Helmy HM, Stumpfl EF, Kamel OA (1995) Platinum-group minerals from the metamorphosed Abu Swayel Cu–Ni–PGE mineralization, South Eastern Desert, Egypt. Econ Geol 90:2350–2360

Hertogen J, Jassens MJ, Palme H (1980) Trace elements in ocean ridge basalts glasses: implications for fractionation during mantle evolution and petrogenesis. Geochim Cosmochim Acta 44:2125–2143

Holwell DA, McDonald I (2006) Partitioning of platinum-group elements in the Platreef at Overysel, northern Bushveld Complex: a combined PGM and LA ICP-MS study. Contrib Mineral Petrol (in press)

Hoffman E, MacLean WH (1976) Phase relations of michenerite and merenskyite in the Pd–Bi–Te system. Econ Geol 71:1461–1468

Hudson DR (1986) Platinum-group minerals from the Kambalda nickel deposits, Western Australia. Econ Geol 81:1218–1225

Kaneda H, Takenouchi S, Shoji T (1986) Stability of pentlandite in the Fe–Ni–Co–S system. Mineral Depos 21:169–180

Kim WS, Chao AG (1991) Phase relations in the system Pd–Sb–Te. Can Mineral 29:401–409

Kingston GA, Eldosuky BT (1982) A contribution on the platinum-group mineralogy of the Merensky reef at the Rustenburg platinum mine. Econ Geol 77:1367–1384

Li C, Barnes S-J, Makovicky E, Rose-Hansen J, Makovicky M (1996) Partitioning of nickel, copper, iridium, rhenium, platinum, and palladium between monosulfide solid solution and sulfide liquid: effects of composition and temperature. Geochim Cosmochim Acta 60:1231–1238

Magyarosi Z, Watkinson DH, Jones PC (2002) Mineralogy of Ni–Cu–platinum-group element sulfide ore in the 825 and 810 orebodies, Copper Clif South Mine, and P–T–X conditions during the formation of platinum-group minerals. Econ Geol 97:1471–1486

Medvedeva ZS, Klochko MA, Kuznetsov AG, Andreyeva SN (1961) Structural diagram of the Pd–Te alloy system (in Russian). Zhurnal Neorganicheskoy Khimii 6:1737–1739

Melcher F, Lodziak J (2006) Platinum-group minerals of concentrates from the Driekop platinum pipe, Eastern Bushveld Complex—tribute to Eugen F. Stumpfl. N Jb Mineral (in press)

Misra KC, Fleet ME (1973) The chemical composition of synthetic and natural pentlandite assemblages. Econ Geol 68:518–539

Mulja T, Mitchell RH (1991) The Geordie Lake intrusion, Coldwell Complex, Ontario: a palladium and tellurium-rich disseminated sulfide occurrence derived from an evolved tholeiitic magma. Econ Geol 86:1050–1069

Naldrett AJ (2004) Magmatic sulfide deposits. Springer, Berlin Heidelberg New York, p 727

Oberthür T, Weiser TW, Gast L, Kojonen K (2003) Geochemistry and mineralogy of platinum-group elements at Hartley Platinum Mine, Zimbabwe. Part 1. Primary distribution patterns in pristine ores of the Main Zone of the Great Dyke. Mineral Depos 38:327–343

O'Neill HSC, Mavrogenes JA (2002) The sulfide capacity and the sulfur content at sulfide saturation of silicate melts at 1400 degrees C and 1 bar. J Petrol 43:1049–1087

Palme H, O'Neill HStC (2003) Cosmochemical estimates of mantle composition, 1–38. In Carlson RW (ed) The mantle and core, Treatise on Geochemistry, Vol 2 (Holland HD Turekian KK eds.), Elsevier, Oxford

Piña R, Gervilla F, Ortega L, Lunar R (2006) Mineralogy and geochemistry of platinum-group elements in the Aguablanca Ni–Cu Deposit (SW Spain). Mineral Petrol (in press)

Prichard HM, Barnes SJ, Maier WD, Fisher PC (2004) Variations in the nature of the platinum-group minerals in a cross-section through the Merensky reef at Impala Platinum: Implications for the mode of formation of the reef. Can Mineral 42:423–437

Rowell WF, Edgar AD (1986) Platinum-group element mineralization in a hydrothermal Cu–Ni sulfide occurrence, Rathbun Lake, northeastern Ontario. Econ Geol 81:1272–1277

Rucklidge J (1969) Electron microprobe investigation of platinum metal minerals from Ontario. Can Mineral 9:617–628

Tarkian M, Koopmann G (1995) Platinum-group minerals in the Santo-Tomas-II (Philex) porphyry copper–gold deposit, Luzon Island, Phillipines. Mineral Depos 30:39–47

Yi W, Halliday AN, Alt JC, Lee D-C, Rehkämper M, Garcia MO, Langmuir CH, Su Y (2000) Cadmium, indium, tin, tellurium, and sulfur in oceanic basalts: implications for chalcophile element fractionation in the Earth. J Geophys Res 105:18927–18948